Catalytic Mechanism and Molecular Recognition of *E. coli* UDP-3-*O*-(*R*-3-Hydroxymyristoyl)-*N*-acetylglucosamine Deacetylase Probed by Mutagenesis†

Marcy Hernick and Carol A. Fierke*

Department of Chemistry, University of Michigan, Ann Arbor, Michigan 48109

Received July 12, 2006; Revised Manuscript Received October 4, 2006

ABSTRACT: UDP-3-*O*-(*R*-3-hydroxymyristoyl)-*N*-acetylglucosamine deacetylase (LpxC) is a metal-dependent deacetylase that catalyzes the hydrolysis of UDP-3-*O*-myristoyl-*N*-acetyl-glucosamine to form UDP-3-*O*-myristoyl-glucosamine and acetate. This is the committed step in the biosynthesis of lipid A, and therefore, LpxC is a target for the development of antimicrobial agents in the treatment of Gram-negative infections. To facilitate the development of potent and specific inhibitors of LpxC, the molecular determinants of binding and specificity and the catalytic mechanism for this enzyme have been probed. The functions of active site residues have been classified on the basis of changes in steady-state turnover (k_{cat}, K_M, and k_{cat}/K_M) and product binding affinity ($K_D^{Product}$). We have identified side chains that enhance product affinity and reactivity (F192, K239, D246, and H265), destabilize product affinity (E78 and D197), and preferentially enhance catalytic efficiency (H19, T19, K143, and N162). In addition, the affinity of LpxC for myrUDP-GlcNH$_2$ is dependent on two ionizations, one deprotonation and one protonation, with apparent pK_a values of 6.5 ± 0.1 and 7.4 ± 0.1, respectively. The UDP moiety of the product contributes significantly to recognition by LpxC, suggesting that this region can be targeted in drug development. These data provide a map of the active site features essential for catalysis and molecular recognition by LpxC that can be used for developing more potent LpxC inhibitors.

The outer membrane of Gram-negative bacteria is comprised of negatively charged lipopolysaccharide (LPS[1]) molecules. Lipid A is the hydrophobic portion of LPS that anchors LPS to the cell wall and is essential for the viability of Gram-negative bacteria (*1*). The enzyme UDP-3-*O*-(*R*-3-hydroxymyristoyl)-*N*-acetylglucosamine deacetylase (LpxC) catalyzes the committed step in the biosynthesis of lipid A, and is, therefore, a target for the development of antibacterial agents, including *Pseudomonas aeruginosa*, *Escherichia coli*, and *Haemophilus influenzae*, in the treatment of Gram-negative infections (*1*−*3*).

LpxC is a metal-dependent deacetylase that catalyzes the conversion of UDP-3-*O*-myristoyl-*N*-acetyl-glucosamine (myrUDP-GlcNAc) to UDP-3-*O*-myristoyl-glucosamine (myrUDP-GlcNH$_2$) and acetate as shown in Figure 1 (*4*). Mutagenesis, pH-dependence and structural studies have been used to examine the mechanism of LpxC leading to the proposals of both single acid−base metalloprotease-like and dual acid−base catalytic mechanisms (*5*, *6*, *27*). The proposed mechanism in Figure 2 employs a metal−water nucleophile and a Glu/His general acid−general base pair that both activates the nucleophile and protonates the amine leaving group (*5*). Other metal-dependent deacetylases are proposed to use a similar catalytic mechanism (*6*).

Efforts toward the development of LpxC inhibitors are underway (*7*−*12*) and will be aided by information regarding the molecular recognition properties and catalytic mechanism of LpxC. Currently, LpxC inhibitors have been identified that contain functional groups capable of chelating the catalytic metal ion, such as hydroxamates, sulfonamides, thiols, phosphonates, and carboxylates (*7*−*12*). Importantly, many of these LpxC inhibitors possess antibacterial activity against several Gram-negative organisms including *E. coli* and *P. aeruginosa* (*7*, *12*). The optimization of metalloenzyme inhibitors both in terms of specificity and potency is well precedented and has been aided by information regarding binding interactions, including enzyme structural data (*2*, *13*−*15*). Our understanding of the features that govern the molecular recognition properties of LpxC are limited to structural data for LpxC from *Aquifex aeolicus* (AaLpxC) (*5*, *16*−*19*), and potential side chains that may be involved in recognition have not been probed biochemically. A more detailed understanding of the structural and electronic features of the active site of LpxC that affect ligand affinity and recognition will facilitate the further development of highly potent and specific LpxC inhibitors.

† This work was supported by the National Institutes of Health (GM40602 to C.A.F.) and the Cystic Fibrosis Foundation (HERNIC05F0 to M.H.).

* To whom correspondence should be addressed. Phone: (734) 936-2678. Fax: (734) 647-4865. E-mail: fierke@umich.edu.

[1] Abbreviations: LPS, lipopolysaccharide; LpxC, UDP-3-*O*-(*R*-3-hydroxymyristoyl)-*N*-acetyl-glucosamine deacetylase; UDP-GlcNAc, uridine-5′-diphosphate-*N*-acetylglucosamine; myrUDP-GlcNAc, UDP-3-*O*-(*R*-3-hydroxymyristoyl)-*N*-acetylglucosamine; myrUDP-GlcNH$_2$, UDP-3-*O*-(*R*-3-hydroxymyristoyl)-glucosamine; EcLpxC, *Escherichia coli* LpxC; AaLpxC, *Aquifex aeolicus* LpxC; BSA, bovine serum albumin; TCEP, triscarboxyethylphosphine; GABC, general acid-base catalyst; UMP, uridine-5′-monophosphate; OPA, *o*-phthaldialdehyde. LpxA, UDP-3-*o*-acyltransferase; CIP, calf intestinal alkaline phosphatase; UDPPGPPase, UDP-glucose pyrophosphonylase.

10.1021/bi061405k CCC: $33.50
Published on Web 12/19/2006

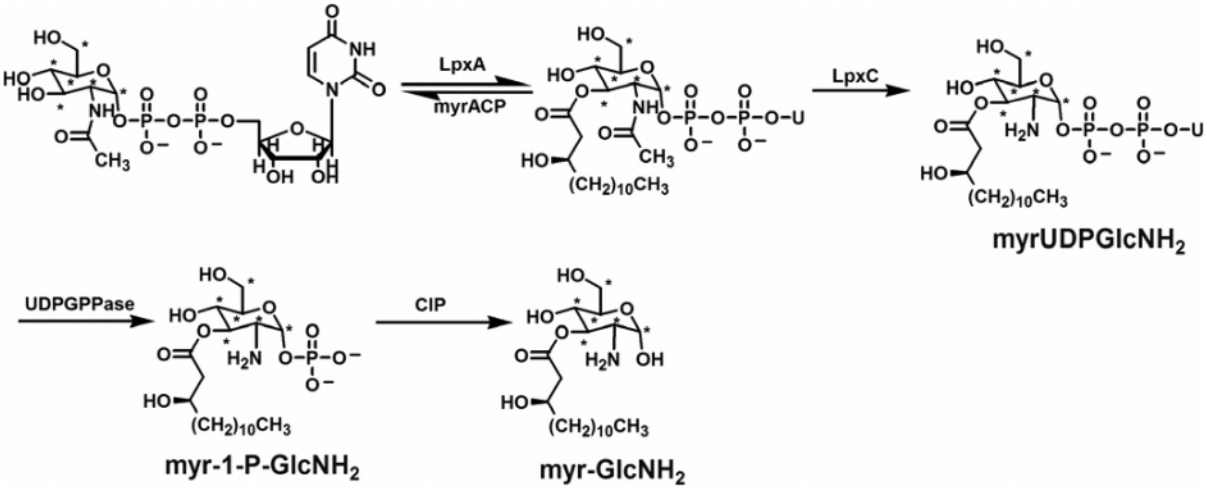

FIGURE 1: LpxC catalyzes the second step in the biosynthesis of lipid A. Product analogues were prepared from the LpxC product, myrUDP-$GlcNH_2$ (see footnote 1 for abbreviations). (*) Denotes the ^{14}C labeled position.

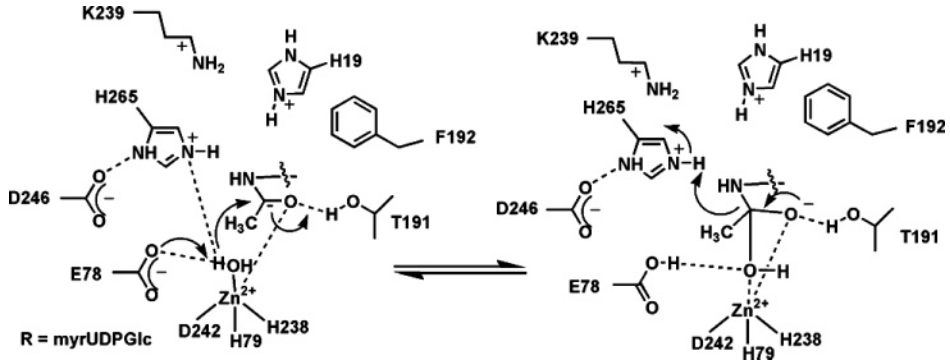

FIGURE 2: Proposed mechanism for LpxC (*5*). The ionization states of side chains and ligands are shown at pH 7, according to their respective pK_a values in the unbound states.

Herein, we analyze features of the active site of *E. coli* LpxC (EcLpxC) that enhance ligand affinity and catalytic activity. The myrUDP-$GlcNH_2$ product binds to EcLpxC with a submicromolar dissociation constant, whereas the product acetate binds weakly (K_D > mM); the UDP moiety contributes ~130-fold to the product binding affinity. Furthermore, the affinity of LpxC for myrUDP-$GlcNH_2$ depends on two ionizations (pK_a values of 6.5 ± 0.1 and 7.4 ± 0.1). Mutagenesis data indicate that the side chains of E78 and H265 act synergistically to enhance product affinity, whereas the conserved residue F192 enhances the affinity of myrUDP-$GlcNH_2$ more than 200-fold, likely due to a C−H/π interaction between the phenyl ring of F192 and the glucosamine moiety of the product. To a lesser extent, the side chain of K239 contributes to product recognition by LpxC and may orient the bound substrate for catalysis. Finally, deletion of the side chains of H19 and T191 decreases the values of k_{cat} and k_{cat}/K_M significantly, with no significant effect on product affinity, suggesting that these residues stabilize the substrate complex and/or the catalytic transition state relative to the product ground state. In light of the structural data, we propose that T191 and H19 stabilize the oxyanion intermediate and flanking transition states. These studies map active site residues in LpxC that are essential for molecular recognition and catalytic activity.

MATERIALS AND METHODS

Mutagenesis and Protein Expression. All mutant plasmids were prepared using Quik-change site-directed mutagenesis kits (Stratagene). LpxC variants were overexpressed and purified according to published procedures using DEAE-sepharose and Reactive Red-120 affinity dye columns (*4*, *12*, *20*, *21*). For the expression of less stable LpxC mutants, the incubation temperature was reduced to 25 °C, following the addition of isopropyl D-thiogalactopyranoside, and cells were incubated overnight. The single zinc bound form of LpxC was prepared according to established procedures (*4*, *5*).

LpxC Deacetylase Assay. [^{14}C]-UDP-3-*O*-(3-hydroxymyristoyl)-*N*-acetyl-glucosamine was prepared, and deacetylase activity was measured as previously described (*4*, *5*, *22*). Briefly, assay mixtures containing 20 mM bis-tris propane at pH 7.5, bovine serum albumin (BSA, fatty acid free, 1 mg/mL), triscarboxyethylphosphine (TCEP, 0.5 mM), and [^{14}C]-UDP-3-*O*-(3-hydroxymyristoyl)-*N*-acetyl-glucosamine were pre-equilibrated at 30 °C, and the reactions were initiated by the addition of the enzyme (0.5 to 5 nM). After incubation for various time periods, the reactions were quenched by the addition of sodium hydroxide, which also cleaves the myristate substituent for ease of separation. Substrate and product were separated on PEI-cellulose TLC plates (0.1 M guanidinium HCl) and quantified by scintillation counting. Initial rates of product formation (<20% reaction) were determined from these data. To evaluate the steady-state kinetic parameters of the EcLpxC mutants, activity was measured at seven to nine different concentrations of myrUDP-GlcNAc (25 nM to 8 μM). The steady-state parameters k_{cat}, K_M, and k_{cat}/K_M were obtained by fitting

the Michaelis−Menten equation to the initial linear velocities measured at the various substrate concentrations using the curve-fitting program Kaleidagraph (Synergy Software), which also calculates the asymptotic standard errors.

Product Analogues. The product analogues [^{14}C]-1-phosphate-3-*O*-(3-hydroxymyristoyl)-glucosamine and [^{14}C]-3-*O*-(3-hydroxymyristoyl)-glucosamine were prepared from [^{14}C]-UDP-3-*O*-(3-hydroxymyristoyl)-glucosamine (Figure 1). [^{14}C]-UDP-3-*O*-(3-hydroxymyristoyl)-GlcNAc (33 μM, 10 mM bis-tris at pH 6) was incubated with EcLpxC (2.4 μM) in 5 mM HEPES at pH 7.5 and 1.8 mM dithiothreitol at 30 °C. After 1 h, LpxC was removed by ultrafiltration (Microcon MWCO 30K), the filter was washed with 100 mM Tris at pH 7.6 (3× 100 μL), and the reaction mixture was concentrated to afford [^{14}C]-UDP-3-*O*-(3-hydroxymyristoyl)-glucosamine (70% yield). TLC confirmed the loss of the *N*-Ac moiety (PEI cellulose, 0.1 M guanidine HCl) as well as the presence of the fatty acid (silica gel, 25:15:4:2 v/v $CHCl_3$/MeOH/H_2O/AcOH) by comparison with known standards. [^{14}C]-UDP-3-*O*-(3-hydroxymyristoyl)-glucosamine (2.4 μM) was then incubated with UDP-glucose pyrophosphorylase from baker's yeast (Sigma, 0.52 units) in 50 mM Tris at pH 7.6, 0.2 mM dithiothreitol, 15 mM $MgCl_2$, and 2.5 mM sodium pyrophosphate at 30 °C (*23*). After 1.5 h, the enzyme was removed by ultrafiltration (Microcon MWCO 30K), the filter was washed with 100 mM Tris at pH 7.6 (2× 100 μL), and the product concentrated using a speed vac. The product [^{14}C]-1-phosphate-3-*O*-(3-hydroxymyristoyl)-glucosamine was purified as described for [^{14}C]-UDP-3-*O*-(3-hydroxymyristoyl)-glucosamine (*4*, *22*). To prepare [^{14}C]-3-*O*-(3-hydroxymyristoyl)-glucosamine, crude [^{14}C]-1-phosphate-3-*O*-(3-hydroxymyristoyl)-glucosamine (∼1.4 μM) was incubated with calf intestinal alkaline phosphatase (NEB, 20 units) in 50 mM Tris at pH 7.6, 1 mM dithiothreitol, 10 mM $MgCl_2$, and 100 mM NaCl at 30 °C (*24*). After 2 h, an additional 2 units of alkaline phosphatase was added to the reaction, and the reaction was incubated at 30 °C for an additional 2 h. The enzyme was removed by ultrafiltration (Microcon MWCO 30K), the filter was washed with 100 mM Tris at pH 7.6 (1× 100 μL), and the resulting product was purified as described for the other analogues (*4*, *22*). Products were confirmed by TLC analysis against known standards (see above; PEI cellulose and silica gel).

Ultrafiltration Binding Assay. Dissociation constants (K_D) for [^{14}C]-UDP-3-*O*-(3-hydroxymyristoyl)-glucosamine, [^{14}C]-1-phosphate-3-*O*-(3-hydroxymyristoyl)-glucosamine, [^{14}C]-3-*O*-(3-hydroxymyristoyl)-glucosamine, uridine-2-[^{14}C] 5′-diphosphate (Sigma), and [^{14}C]-acetate (American Radiolabeled Chemicals, Inc.) from EcLpxC−ligand complexes were measured using ultrafiltration. In these experiments, the concentration of product, or product analogue, was held constant (below the K_D value, ≤73 nM), and the concentration of the enzyme was varied (0 to 230 μM). The enzyme and substrate/products were incubated at 30 °C for 15−30 min prior to the assay to allow for product formation and/or ligand equilibration. Assay mixtures were then transferred into ultrafiltration devices (Microcon MWCO 30K), and the free and bound products were separated by centrifuging the samples at 3000 rpm for 2.5 min. Control experiments show that each of the ligands, but not LpxC, readily crosses the membrane. No more than 20% of the assay volume goes through the membrane, ensuring that equilibrium conditions are not significantly perturbed during the course of the experiment. Equal volumes of the filtrate and retentate were removed, and the amounts of unbound (filtrate) and total product (retentate) were quantified using scintillation counting. The ratio of EP/P_{total} was determined as a function of $[E]_{total}$, and the K_D values were obtained by fitting eq 1 to these data. For ligands that have low affinity for LpxC, K_D values were estimated by fixing the EP to that measured for myrUDPGlcNH$_2$ ($EP/P_{total} = 0.9$). These experiments were performed at various pH values in the range of 5−9.8 (25 mM buffer, 1.5 mM TCEP; MES, pH 5−6.5; bis-tris propane, pH 7−9.8), and the pK_a values were determined using eq 2. Equation 2 was derived from a thermodynamic box describing product binding to an enzyme containing two ionizable groups. When $K_{a2}/K_{a3} \ll 1$, this term drops out of the equation, and the simplified version of eq 2 was fit to the data. Inclusion of additional ionizations into eq 2 decreases the goodness of the fits, indicating that the data are best described by two ionizations. For mutants that bind product weakly (i.e., F192A, D246A, and H265A), accurate determinations of pK_a values were not possible, and therefore, K_D values at the pH minima (K_D value at pH with highest affinity) are reported in Table 2. To probe whether the recognition properties of LpxC for the product are similar for AaLpxC and EcLpxC, $K_D^{Product}$ values were determined for WT AaLpxC and AaK227A at pH 7.5 and compared to the values obtained for the corresponding EcLpxC variants (WT, EcK239A).

Table 1: Steady-State Parameters for Deacetylation Catalyzed by *E. coli* LpxC

E. coli LpxC[a,b]	k_{cat} (min^{-1})	K_M (μM)	k_{cat}/K_M ($\mu M^{-1}min^{-1}$)	fold-decrease (k_{cat}/K_M)
WT−Zn^{2+}[c]	90 ± 2	0.19 ± 0.01	460 ± 10	
H19A	1.0 ± 0.1	1.3 ± 0.3	0.8 ± 0.1	575
H19Y	15 ± 4	11 ± 4	1.3 ± 0.1	350
H19Q	8 ± 1	2.4 ± 0.6	3.4 ± 0.3	135
K143A[d]	N/A	N/A	0.6	700
N162A[d]	N/A	N/A	0.4	1200
T191A	3.2 ± 0.4	1.6 ± 0.5	2.0 ± 0.4	230
F192A	0.31 ± 0.07	0.5 ± 0.3	0.7 ± 0.3	660
D197E	79 ± 6	0.8 ± 0.1	100 ± 7	5
D197A	90 ± 30	1.1 ± 0.6	85 ± 20	5
K239A[d]	0.6 ± 0.1	0.8 ± 0.2	0.8 ± 0.1	575

[a] The metal-substituted enzymes were prepared with a stoichiometry of 1:1 as described in Materials and Methods. [b] The initial rate for LpxC-catalyzed deacetylase activity was determined at 30 °C (20 mM bis-tris propane at pH 7.5, 1 mg/mL BSA, and 0.5 mM TCEP) with the substrate myrUDP-GlcNAc. The kinetic parameters were obtained from the initial velocities as described in Materials and Methods. [c] Data taken from ref 5 for comparison purposes. [d] Substrate inhibition observed at [S] > 0.1 (K143A, N162A) or 1 μM (K239A). The activity of K143A and N162A mutants was calculated from the initial linear portion of the curves assuming no substrate inhibition.

$$\frac{EP}{P_{total}} = \frac{(EP/P_{total})_{Endpt}}{\left(1 + \frac{K_D}{E_{total}}\right)} + (EP/P_{total})_{Background} \quad (1)$$

$$K_{D,app} = K_D\left(1 + \frac{[H]}{K_{a1}} + \frac{K_{a2}}{[H]} + \frac{K_{a2}}{K_{a3}}\right) \quad (2)$$

Potentiometric Titrations. The pK_a values for the ionizable groups of the model compounds glucosamine and UDP-

Table 2: Affinity of EcLpxC Mutants for myrUDP-GlcNH$_2$

E. coli LpxC[a,b,c]	pK_{a1}	pK_{a2}	K_D (μM)[d]	fold-increase[e]
WT−Zn^{2+}	6.5 ± 0.1	7.4 ± 0.1	0.64 ± 0.1	
E78A	7.2 ± 0.2	6.9 ± 0.2	0.03 ± 0.01	0.05 (23)
F192A	[f]	[f]	146 ± 20	228 (2.6)
D197E	6.2 ± 0.2	8.3 ± 0.2	0.14 ± 0.02	0.22 (4)
K239A	6.5 ± 0.2	7.2 ± 0.2	3.5 ± 1.4	6 (4)
D246A	[f]	[f]	28 ± 7	44 (1.3)
H265A	[f]	[f]	26 ± 3	41 (7)
E78A/H265A	[f]	[f]	22 ± 5	34 (10)

[a] The metal-substituted enzymes were prepared with a stoichiometry of 1:1 as described in Materials and Methods. [b] The K_D values were determined at 30 °C (25 mM buffer and 0.5 mM TCEP at pH 5−9.8) as described in Materials and Methods. [c] Mutations that alter $K_D^{Product}$ ≤ 2-fold are not listed in the Table, including Co-WT, H19A, H19Y, H19Q, K143A, N162A, T191A, and D197A. [d] The pH independent K_D values are calculated using eq 2. [e] The effects of these mutations on K_M at pH 7.5 (from Table 1 or ref 5) are shown in parentheses. [f] The affinity was too weak to accurately determine pK_a values; therefore, the K_D value at the pH minima is reported (F192A at pH 7; D246A at pH 7.5; H265A at pH 6; E78A/H265A at pH 8.5).

GlcNAc were determined using potentiometric titrations. In these experiments, glucosamine (4.5 mM, 20 mL) in 0.15 M NaCl was titrated with 0.1 M NaOH in the pH range 5.4 to 11 (110 increments) and the pH measured using an Orion research digital pH meter model 611 at 25 °C. UDP-GlcNAc (4.5 mM, 20 mL) was dissolved in 0.15 M NaCl and the pH adjusted to 1.68 using 1 M HCl. The solution was titrated with 0.1 M NaOH in the pH range of 1.68 to 12.00 (146 increments). The pH values at the equivalence points were determined from first and second derivative plots and are equal to the pK_a values (*25*).

pK_a Determination of Amines. The pK_a values for product amine groups were determined by examining the rate of reaction with the reagent *o*-phthaldialdehyde (OPA, Molecular Probes). OPA itself is not fluorescent; however, it reacts with primary amines in the presence of thiols to form a fluorescent product (Ex 344 nm, Em 455 nm), and the observed rate constant is dependent on the concentration of deprotonated amine (*26*). The rates of reaction of the primary amines glucosamine, UDP-glucosamine, and myrUDP-glucosamine with OPA at various pH values were measured and the pK_a values determined from the pH dependence of these rates. UDP-GlcNH$_2$ and myrUDP-GlcNH$_2$ were obtained by reacting the corresponding *N*-Ac compounds with LpxC, followed by the removal of LpxC using ultrafiltration (Microcon, MWCO 30K). Reactions were initiated by the addition of the primary amine (~20 μM) to a cuvette containing OPA (7.46 mM), 2-mercaptoethanol (1.44 mM), and 20 mM buffer (see below). The increase in fluorescence (Ex 344 nm, Em 455 nm) over 2 min was monitored, and the rate constants were calculated by fitting an exponential equation to the resulting data. The pK_a values were obtained by fitting eq 3 to the pH dependence of the observed rate constants, where k_1 is the pH independent rate constant for the reaction of amine with OPA at high pH, and k_2 is the background rate constant. The buffers used in these experiments were MES at pH 5.45−6.52; bis-trispropane at pH 7.06−9.58; and CAPS at pH 9.97−10.67.

$$k_{obs} = \frac{k_1}{(1 + 10^{pKa-pH})} + k_2 \qquad (3)$$

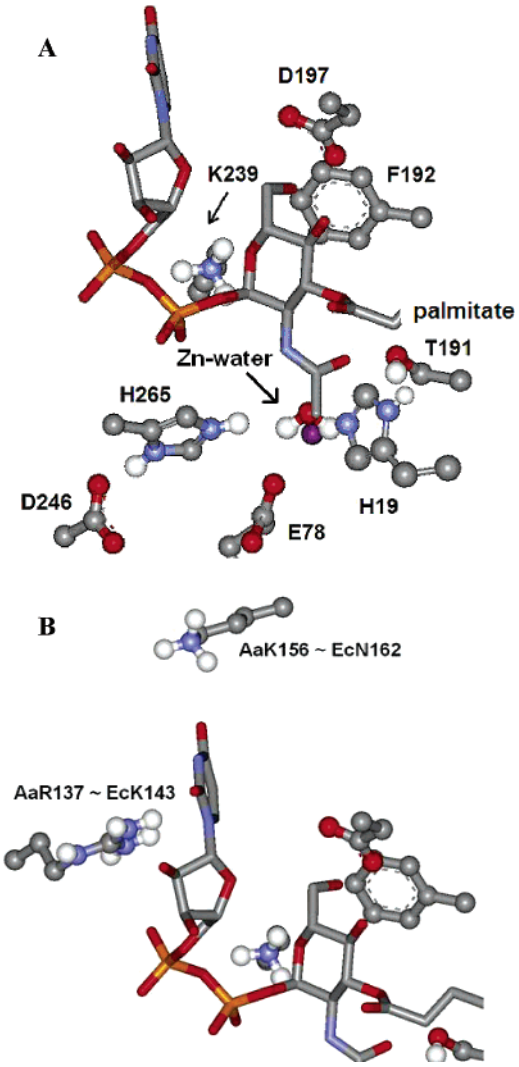

FIGURE 3: Active site of *A. aeolicus* LpxC with modeled substrate PDB 1P42 (*16*). For clarity, *E. coli* LpxC numbering is used unless otherwise stated.

RESULTS

Steady-State Turnover of Mutants. To further our understanding of the molecular recognition properties and catalytic mechanism of EcLpxC, we used site-directed mutagenesis to identify side chains that are important for high affinity ligand binding and/or efficient catalysis. There are currently no structural data available for EcLpxC. Therefore, amino acid side chains that may contribute to molecular recognition were identified from a model of substrate bound to the active site of AaLpxC (*16*) (Figure 3). There is ~30% sequence homology between LpxC from *A. aeolicus* and *E. coli*; however, a higher degree of conservation is exhibited for the residues that line the active site. The residues examined here, except for K143 and N162, are conserved across all known LpxC variants. The side chains of E78, T191, and H265 are located near the catalytic zinc ion (≤5 Å) (*5*, *27*), and in the current mechanism, Glu78 and His265 are proposed to function as a general acid−base catalyst pair. In addition, D246 is part of a His−Asp charge relay with H265, and the side chain of T191 is proposed to stabilize the oxyanion intermediate and flanking transition states (Figure 2) (*5*). The side chain of K239 has also been suggested to stabilize the negatively charged oxyanion of

the tetrahedral intermediate (*27*). Additionally, the side chains of K143 (Aa R137), N162 (Aa K156), and K239 are all positioned within hydrogen-bonding distance of the UDP moiety (Figure 3), whereas the side chains of F192 and D197 (conserved charge) surround the glucose portion of the substrate, and H19 lies at the base of the hydrophobic tunnel near the *N*-acetyl group of the substrate. Consequently, these side chains have the potential to influence molecular recognition by LpxC.

The effects of Ala mutations at each of these positions on the steady-state parameters k_{cat}, K_M, and k_{cat}/K_M were determined (20 mM bis-tris propane at pH 7.5, 1 mg/mL BSA, 0.5 mM TCEP; Table 1). Remarkably, Ala substitutions at positions H19, K143, N162, T191, F192, and K239 all cause large decreases (230- to 700-fold) in k_{cat}/K_M, indicating that these side chains are important for catalytic efficiency by enhancing substrate affinity and/or stabilizing the catalytic transition state. Previously, the side chain of T191 was proposed to stabilize a tetrahedral intermediate and flanking transition states through hydrogen-bonding interaction(s) on the basis of the crystal structure of the AaLpxC−cacodylate (mimics tetrahedral intermediate) complex (*5*). Additionally, a hydrogen bond is observed between the side chain of T191 and the carbonyl oxygen of TU-514 (hydroxamate inhibitor), further supporting this hypothesis (*19*). The decrease in k_{cat}/K_M (230-fold) that is observed for T191A is consistent with this role for T191 in catalysis. An even larger decrease in k_{cat}/K_M (590-fold) is observed for the H19A mutant; however, structural data suggest that the side chain of H19 is too far away (≥5 Å) to directly hydrogen bond with the oxygen atom of the oxyanion intermediate (*5*, *16*−*19*). Substitution of H19 with Gln, which retains hydrogen-bonding ability, and Tyr, as observed in the *E. coli* chromosomal mutant defective in lipid A formation (*20*, *28*), also decreases k_{cat}/K_M more than 130-fold. These findings suggest that the positive charge and/or size of the side chain are more important for efficient catalytic activity than simple hydrogen-bonding interactions. Unexpectedly, k_{cat}/K_M decreases 700-fold in the F192A mutant, indicating that this side chain contributes significantly to catalytic efficiency. Because F192 contains no polar groups that could participate directly in the catalytic mechanism, it is likely that this effect on k_{cat}/K_M is mediated through an effect on substrate affinity and/or positioning.

Interestingly, the K143A and N162A LpxC mutants exhibit a large degree of substrate inhibition at [S] > 0.1 μM; therefore, the values of k_{cat}/K_M for these mutants were estimated from the initial linear dependence of rate on substrate concentration. Both of these mutations decrease catalytic efficiency (k_{cat}/K_M) more than 575-fold. The side chains K143 and N162 are located in the UDP binding pocket (Figure 3), far from the catalytic Zn(II) (15−20 Å), and are, therefore, likely to be important for substrate affinity and/or positioning. The observed substrate inhibition may be a consequence of the nonproductive binding of a second substrate molecule.

All of the mutations examined also increase K_M, suggesting either that all of the mutations decrease substrate affinity (if $K_M = K_D^{substrate}$) or that K_M for WT LpxC is kinetically lowered (if $K_M \leq K_D^{substrate}$). For mutants with significantly lowered values of k_{cat}, it is likely that $K_M \approx K_D^{substrate}$. Alanine substitutions for H19, T191, F192, and K239 in EcLpxC decrease the value of k_{cat} by 30- to 1000-fold (Table 1). These mutations also generally decrease the product affinity (Table 2), suggesting that product dissociation is not a main rate-contributing step in turnover. Therefore, the decreases in k_{cat} suggest that these side chains stabilize the hydrolytic transition state relative to the ground state E−S complex. If product dissociation is the rate-limiting step for the wild-type enzyme, then these decreases represent a lower limit for the stabilization of the catalytic transition state by these residues.

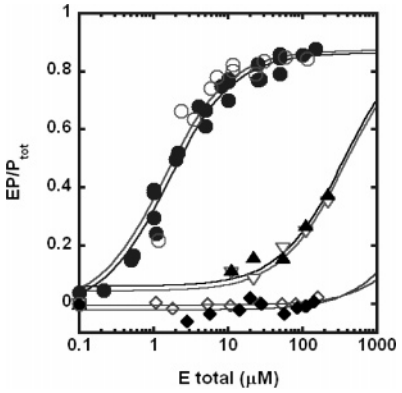

FIGURE 4: Product binding (●) myrUDP-GlcNH$_2$, (▲) myr-1-P-GlcNH$_2$, (▽) myrGlcNH$_2$, (♦) UDP, and (◊) acetate to EcLpxC, and (○) myrUDP-GlcNH$_2$ binding to AaLpxC measured by ultrafiltration in 20 mM bis-tris propane and 1.5 mM TCEP at pH 7.5.

Product Affinity of EcLpxC. To further explore the molecular recognition properties of LpxC, we measured the K_D values of the products myrUDP-GlcNH$_2$ and acetate (Figure 1) for EcLpxC at pH 7.5 (Table 2 and Figure 4). Because the hydrolytic reaction is essentially irreversible, thermodynamic dissociation constants can be directly measured. The product myrUDP-GlcNH$_2$ binds to EcLpxC with a K_D value of 1.5 ± 0.2 μM at pH 7.5, which is ~8-fold higher than the value of the substrate K_M (Table 1). In contrast, less than 2% of [^{14}C]-acetate binds to 150 μM LpxC, indicating that the $K_D^{Acetate}$ value is large (≥8 mM). Together, these data suggest that the acetyl moiety contributes only modestly to substrate binding affinity. In addition, the affinity of AaLpxC for myrUDP-GlcNH$_2$ is within error the same as that of EcLpxC with a $K_D^{Product}$ value[2] of 1.8 ± 0.6 μM, suggesting that the major interactions governing the recognition of myrUDPGlcNH$_2$ by LpxC are similar for both enzymes.

The role of the UDP moiety in molecular recognition of myrUDP-GlcNH$_2$ by EcLpxC was probed by examining the affinity of UDP as well as the product analogues 1-phosphate-3-*O*-(3-hydroxymyristoyl)-glucosamine and 3-*O*-(3-hydroxymyristoyl)-glucosamine (Figure 1). At 140 μM LpxC, less than 5% of the [^{14}C]-UDP binds to LpxC, indicating that the K_D^{UDP} value is higher than 5 mM (<4 kcal/mol binding energy). This result is consistent with previous NMR data, suggesting that AaLpxC binds UDP and UMP weakly (*18*). However, deletion of the UMP or UDP moieties in the product analogues increases the value of K_D from 1.5 to ~200 μM, demonstrating that the UDP moiety contributes about 130-fold (2.9 kcal/mol) to the overall binding affinity (8.0

[2] $K_D^{Product}$ refers to the dissociation constant for an EcLpxC−myrUDPGlcNH$_2$ complex.

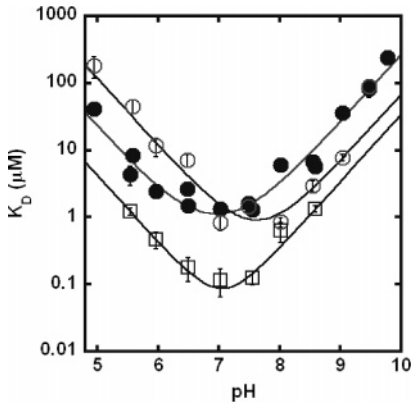

FIGURE 5: pH dependence of the K_D for myrUDP-GlcNAc dissociating from a complex formed with (●) Zn-WT, (○) Co-WT, and (□) Zn-E78A EcLpxC.

kcal/mol) of myrUDP-$GlcNH_2$, consistent with the observed affinity of UDP alone.

pH Dependence of myrUDP-$GlcNH_2$ Binding to EcLpxC. The affinity of EcLpxC for the product (myrUDP-$GlcNH_2$) was determined as a function of pH to ascertain whether there are ionizations important for binding affinity. For WT LpxC, the $K_D^{Product}$ value increases at both low and high pH in a log-linear fashion, indicating that two ionizations affect binding affinity (Figure 5). The simplest interpretation of these data is that deprotonation of a group with a pK_{a1} of 6.5 ± 0.1 and protonation of a group with a pK_{a2} of 7.4 ± 0.1 both contribute to maximal product affinity. The pK_a values observed in product affinity could reflect ionizations in either, or both, the ligand or the enzyme.

pK_a Values of myrUDP-$GlcNH_2$. There are several ionizable groups in the product myrUDP-$GlcNH_2$ that could be responsible for the observed ionizations in LpxC affinity. Therefore, the pK_a values of these groups were estimated. The pK_a value of the product amine can be estimated from the pK_a value of the amine group in glucosamine, which was determined from potentiometric titrations to be 7.6 ± 0.1, in agreement with the published value of 7.8 (*29*). To investigate whether the fatty acid and UDP moieties significantly alter this pK_a, we determined the amine pK_a values of UDP-$GlcNH_2$ and myr-UDP-$GlcNH_2$ from the pH dependence of the rate constant for the reaction of the amine with *o*-phthaldialdehyde (OPA). For UDP-$GlcNH_2$ and myrUDP-$GlcNH_2$, the pH dependence of the rate constant can be described by a single ionization that enhances reactivity (pK_a = 7.9 ± 0.2; data not shown). Additionally, the value of this pK_a implies that ionization of the amine is not the origin of pK_{a1} but could be reflected in pK_{a2}.

The pK_a values for the diphosphate moiety of myrUDP-$GlcNH_2$ were estimated from those measured in UDP-GlcNAc, where potentiometric titrations (data not shown) indicate that the pK_a values of the diphosphate are ~2 and 7.5, consistent with the pK_a values of other sugar diphosphates (*30*). Again, these results rule out ionization of the diphosphate as the source of pK_{a1} but suggest that ionization of the diphosphate group may be reflected in pK_{a2}.

Structural Changes that Affect the Affinity of Product Binding. To identify specific groups in LpxC that contribute to product (myrUDP-$GlcNH_2$) binding affinity, we altered the active site metal ion and key active site residues (*16*) (Figure 3) and measured product affinity as a function of pH. Specifically, we measured the affinity of myrUDP-$GlcNH_2$ for EcLpxC containing an Ala substitution at the following residues (Table 2): H19, E78, K143, N162, T191, F192, D197, K239, D246 and H265 as well as H19Y, a mutation found in the LpxC strain *envA1*, which displays decreased LpxC activity (*20*, *31*, *32*). The largest decreases in maximal affinity (30- to 225-fold) are observed for the F192A, D246A, and H265A mutations, suggesting that interactions with the F192, D246, and H265 side chains enhance product binding affinity, likely through direct contacts with the bound ligand. A more modest decrease in product binding affinity (6-fold) is observed for the K239A mutation; the corresponding AaLpxC mutation, AaK227A, also decreases the $K_D^{Product}$ value 5-fold, suggesting that this side chain has a similar interaction with the product bound for both EcLpxC and AaLpxC.

Unexpectedly, mutations at multiple positions enhance product affinity. The EcE78A mutant increases the affinity of the product by 20-fold, indicating that the product bound to WT LpxC is strained. Alteration of other active site amino acids also modestly enhances product affinity (2- to 3-fold), including the H19Q/Y and D197A/E mutations, suggesting that these groups do not play an important role in molecular recognition by LpxC. Changes in the active site metal ion and the deletion of active site side chains also alter the observed ionizations in product affinity (Table 2), which will be discussed below.

DISCUSSION

The effects of the mutations on the steady-state kinetic parameters (k_{cat}, K_M, and k_{cat}/K_M) and thermodynamic data ($K_D^{Product}$) can be analyzed in light of specific structural contacts. This analysis assumes that the observed changes in LpxC activity and product affinity for the mutants are not simply due to changes in the global structure of the enzyme. The finding that all of the mutants examined have comparable affinity (≤3-fold change) for a fatty acid analogue compared to that of WT EcLpxC (*39*) suggests that the global structures of these enzymes are not significantly perturbed from that of WT, although local structural changes in the active site cannot be ruled out.

Side Chains Stabilize Both the Bound Product and the Catalytic Transition States. For the F192A, K239A, D246A, and H265A mutants, $K_D^{Product}$ is increased (6−225-fold), whereas k_{cat}/K_M and k_{cat} are decreased (150−2200-fold). The F192A, D246A, and H265A mutations have large effects on $K_D^{Product}$ and k_{cat}/K_M compared to that on K_M (Tables 1 and 2), suggesting that these side chains enhance product binding affinity and transition state stability. These side chains likely directly interact with the product and stabilize the formation of the product, possibly by stabilizing the tetrahedral intermediate or leaving group(s). Although the importance of the H265 and D246 side chains to the catalytic mechanism has been discussed elsewhere (Figure 2 (*5*)), the effects on $K_D^{Product}$ suggest that the H265 and D246 side chains also contribute to molecular recognition by LpxC. In the structural model of substrate bound to AaLpxC (Figure 2), His265 is located near the diphosphate of the UDP moiety and likely forms a hydrogen bond or electrostatic interaction with this group to enhance product affinity. The effect of altering the D246 side chain is likely mediated through an effect on the position or charge of H265.

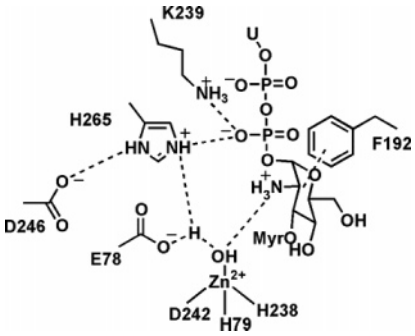

FIGURE 6: Proposed model for binding contacts. The ionization states of side chains and ligands are shown at pH 7, according to their respective pK_a values in the unbound states.

The mutation of F192 to Ala leads to the largest increase in $K_D^{Product}$ (>200-fold; >3 kcal/mol). We propose that this effect is mediated through a C−H/π interaction between the phenyl ring of F192 and the glucosamine moiety of the product that contributes to the molecular recognition of LpxC. C−H/π stacking interactions are common among enzymes that bind sugar molecules (glucose, galactose, mannose, etc.) and contribute to the molecular recognition of these enzymes (*33*−*35*). A more modest decrease in product binding affinity is observed for the K239A mutation; in this case, the increases in $K_D^{Product}$ and K_M are comparable (~5-fold), suggesting a similar interaction of this residue with both product and substrate. The position of this residue (Figure 3) suggests that the K239 side chain may also interact with the diphosphate group on product and substrate. A hydrogen bond between K239 and the diphosphate group of UDP is observed in the crystal structure of an AaLpxC−UDP complex (Gennadios, H., and Christianson, D. W. (2006) Binding of Uridine 5′-Diphosphate in the "Basic Patch" of the Zinc Deacetylase LpxC and Implications for Substrate Binding, *Biochemistry*, 15216-15223), further supporting this hypothesis. Deleting this side chain decreases catalytic efficiency (k_{cat}/K_M) ~100-fold more than the product or substrate affinity, implying that K239 also stabilizes the catalytic transition state relative to that of the E−S complex, either by orienting the substrate optimally for reaction or by stabilizing the developing charge on the leaving group.

Side Chains that Destabilize Product Affinity. Deletion of the D197 and E78 side chains enhances the affinity of the product relative to that observed for WT LpxC ($\Delta\Delta G$[3] = −0.5 and −1.8 kcal/mol, respectively), indicating that these side chains destabilize the product affinity of WT LpxC. Increased K_M values are also observed for both the D197A and E78A mutants, suggesting that these side chains enhance substrate binding, assuming that $K_M \approx K_D^S$. The simplest explanation of these data is that the side chains of these residues interact favorably with the *N*-Ac group of the substrate and/or unfavorably with the amino moiety of the product. Alternatively, the bound substrate and product may occupy different positions in the enzyme leading to differential interactions.

Structural data demonstrate that the side chain of E78 forms a hydrogen bond with the zinc−water (Figure 6), where it is proposed to function as a general base catalyst (*5*, *27*) and may also enhance substrate affinity by forming a hydrogen bond to the NH of the *N*-acetyl moiety either directly or via a water molecule. The enhanced product affinity in the E78A mutant implies that the negatively charged carboxylate decreases product affinity despite the potential for a favorable charge interaction with a positively charged amine in the product. The destabilization of product binding by E78 suggests that this side chain may also function to facilitate product release in WT LpxC. In contrast, the E78A mutation causes the value of K_M to increase by 8-fold (*5*). These data suggest that this side chain has differential effects on ligand affinity during the catalytic cycle, stabilizing the bound substrate but destabilizing the bound product.

In the crystal structure of the AaLpxC−TU-514 (hydroxamate inhibitor) complex and model of the AaLpxC−substrate complex, the side chain of D197 is positioned to hydrogen bond with the hydroxyl groups on the glucose moiety (2.4−3.3 Å), which would presumably enhance substrate affinity (*16*, *19*). However, product affinity is destabilized by the D197 side chain, suggesting that these hydrogen bonds are broken, or become nonoptimal, in the product complex. One possibility is that loss of this hydrogen bond allows for movement of the ligand closer to the metal−water to optimize this interaction during the course of the reaction.

Two Ionizations Contribute to Product Recognition. The pH dependence of product affinity (Figure 5) indicates that two ionizations are required for maximal binding affinity, one deprotonation and one protonation with apparent pK_a values of 6.5 and 7.4, respectively. Although groups on the product have pK_a values similar to those of pK_{a2}, the finding that mutations in the enzyme alter the values of both pK_a's suggests that both ionizations represent groups on the enzyme. It is likely that neither of these ionizations are coupled to protein unfolding because the affinity of a fatty acid ligand shows little pH dependence over this range (*39*). Although the current data do not allow a definitive determination of the identity of the ionizing groups because all of the mutants retain two ionizations, they do provide intriguing clues. Substitution of the active site Zn(II) with Co(II) leads to an increase in the pK_{a1} value, suggesting that pK_{a1} represents a metal-dependent ionization. This pK_a value could either reflect ionization of the metal−water ligand or a group that hydrogen bonds with the metal−water ligand (such as E78). The pK_a values of two LpxC side chains have previously been determined (E78 pK_a 6.2 (*5*, *27*), H265 pK_a 7.6 (*18*)) and are similar to the pK_a values observed for product binding to EcLpxC, leading to speculation that the ionization of these groups cause the observed pH dependence of product affinity.

E78 and H265 Act Synergistically to Bind Product. A comparison of the properties of the single (E78A and H265A) and double E78A/H265A mutants demonstrates that the effects of these single mutations on product affinity are NOT additive (Figure 7). The H265A mutation decreases product affinity ($\Delta\Delta G$ = 2.2 kcal/mol), whereas the E78A mutation enhances product affinity ($\Delta\Delta G$ = −1.8 kcal/mol) relative to WT LpxC. If these two residues act independently of one another to facilitate product binding, the effects of these two mutations should be additive, and the product affinity of the E78A/H265A double mutant should be comparable to that

[3] $\Delta\Delta G_{kcat} = -RT \ln(k_{cat}^{mutant}/k_{cat}^{WT})$; $\Delta\Delta G_{Kd} = -RT \ln(K_D^{mutant}/K_D^{WT})$; $\Delta\Delta G_{Km} = -RT \ln(K_M^{mutant}/K_M^{WT})$.

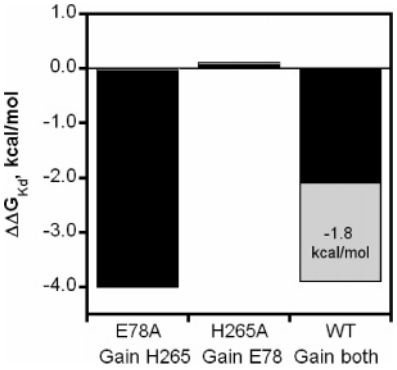

FIGURE 7: Synergy between E78 and H265 for stabilizing product affinity.

of WT LpxC ($\Delta\Delta G$ = 0.4 kcal/mol). In contrast, product affinity for the E78A/H265A mutant is comparable to the H265A mutant and weaker ($\Delta\Delta G$ = 2.1 kcal/mol) than that predicted for additive mutations, indicating that the side chains of H265 and E78 synergistically facilitate product binding.

To analyze the cooperative effects of E78 and H265, we started with the mutant that has both side chains deleted (E78A/H265A) and examined the effects that restoring individual side chains have on product affinity (Figure 7). This analysis provides information regarding the intrinsic, non-cooperative interactions of individual side chains because it begins with an unstrained E−product complex (*36*, *37*). The addition of the H265 side chain provides a large, favorable interaction with the product (−4.0 kcal/mol), whereas the addition of the E78 side chain has a small, unfavorable interaction (0.1 kcal/mol) with the product. The addition of both side chains has a smaller effect than that of the individual single side chains (−2.1 kcal/mol), indicating that E78 and H265 interact in an anticooperative manner to bind the product (*36*, *37*) and that strained product binding in WT is responsible for the observed energy difference (1.8 kcal/mol). Similar findings have been reported for staphylococcal nuclease, wherein an Arg and Glu GABC pair bind substrate in an anticooperative manner (*38*).

Implications for Catalytic Activity. All of the mutations examined alter the steady-state parameters (k_{cat}/K_M, k_{cat}, and K_M) of LpxC, indicating that the side chains of these residues are important for catalysis. Notably, there is an inverse correlation between the value of k_{cat} and the value of $K_D^{Product}$ for many of the mutants; as $K_D^{Product}$ increases, the value of k_{cat} decreases (Tables 1 and 2). This correlation suggests that a step other than product release, such as deacetylation, is the predominant rate-contributing step in k_{cat} for the mutants examined. If product dissociation was the rate-limiting step in k_{cat}, the opposite correlation would be predicted: an increase in the dissociation constant should lead to an increase in the dissociation rate constant, and hence, k_{cat} should increase.

Mechanistically, one of the most significant findings from these studies is that the value of k_{cat}/K_M and k_{cat} are decreased 230-fold ($\Delta\Delta G^{\ddagger}$ = 3.3 kcal/mol) and 30-fold ($\Delta\Delta G^{\ddagger}$ = 2 kcal/mol), respectively, for the T191A mutation. These decreases are much larger than the changes observed in either K_M (7−8-fold) or $K_D^{Product}$ (<2-fold), suggesting that the T191 side chain specifically stabilizes the transition state, consistent with the proposed mechanism wherein this residue stabilizes the tetrahedral intermediate and flanking transition states in the reaction (*5*). This is the first biochemical evidence to support the involvement of T191 in the chemical mechanism of LpxC. The preferential effect of T191 on lowering the value of K_M, which may reflect K_D^S, compared to the value of $K_D^{Product}$ is consistent with T191 forming a hydrogen bond with the carbonyl oxygen of the *N*-acetyl group on the bound substrate, an oxygen atom that is not present on the product.

Similarly, the H19A mutation significantly decreases k_{cat}/K_M (590-fold) and k_{cat} (90-fold) and increases K_M (7-fold) more than $K_D^{Product}$. These data imply that H19 stabilizes the transition state relative to the E−S ground state. Because H19 is positioned at the base of the hydrophobic tunnel next to the *N*-Ac group in the E−S complex model and the myristoyl carbonyl group in the E−TU-514 complex, this side chain may assist in orienting the substrate for catalysis. The positively charged His may also stabilize the negatively charged tetrahedral intermediate, especially if the position of the substrate alters during the course of the reaction.

Implications for Drug Design. Structural information for LpxC is only available for LpxC from *A. aeolicus*; however, interest in the development of inhibitors is focused on LpxC from different pathogenic organisms. The $K_D^{Product}$ values for WT are similar for both AaLpxC and EcLpxC, whereas comparable changes in binding affinity are observed for several mutations, suggesting that the recognition of the product by AaLpxC and EcLpxC is similar. Therefore, structural information for AaLpxC can be used as a starting point for probing the recognition properties of LpxC from other sources.

Previous findings on molecular recognition by LpxC have focused on the incorporation of functional groups to target the hydrophobic tunnel and catalytic metal ion for optimal binding affinity in drug design (*16*, *18*, *19*, *39*, *40*). Our data indicate that additional inhibitor affinity, and possibly specificity, may be obtained by targeting the UDP pocket and ionizing groups in the active site, including H265 and K239. The UDP moiety provides 2.9 kcal/mol to product binding affinity, demonstrating the importance of this group for recognition. Furthermore, the proposed interaction between the glucosamine moiety and the phenyl ring of F192 could be targeted to enhance inhibitor affinity, as observed for product affinity. Taken together, these findings suggest several additional interactions with LpxC that could be targeted to further enhance the potency of LpxC inhibitors.

ACKNOWLEDGMENT

We thank David Christianson and Heather Gennadios (University of Pennsylvania) for helpful discussions, Christian Raetz (Duke University) for supplying the LpxA plasmid, and James Hougland and Nathan Zahler (University of Michigan) for helpful comments on this manuscript.

REFERENCES

1. Raetz, C. R. H., and Whitfield, C. (2002) Lipopolysaccharide endotoxins, *Annu. Rev. Biochem. 71*, 635−700.
2. White, R. J., Margolis, P. S., Trias, J., and Yuan, Z. Y. (2003) Targeting metalloenzymes: a strategy that works, *Curr. Opin. Pharmacol. 3*, 502−507.
3. Onishi, H. R., Pelak, B. A., Gerckens, L. S., Silver, L. L., Kahan, F. M., Chen, M. H., Patchett, A. A., Galloway, S. M., Hyland, S. A., Anderson, M. S., and Raetz, C. R. H. (1996) Antibacterial agents that inhibit lipid A biosynthesis, *Science 274*, 980−982.

4. Jackman, J. E., Raetz, C. R. H., and Fierke, C. A. (1999) UDP-3-O-(R-3-hydroxymyristoyl)-N-acetylglucosamine deacetylase of Escherichia coli is a zinc metalloenzyme, *Biochemistry 38*, 1902−1911.
5. Hernick, M., Gennadios, H. A., Whittington, D. A., Rusche, K. M., Christianson, D. W., and Fierke, C. A. (2005) UDP-3-O-((R)-3-hydroxymyristoyl)-N-acetylglucosamine deacetylase functions through a general acid-base catalyst pair mechanism, *J. Biol. Chem. 280*, 16969−16978.
6. Hernick, M., and Fierke, C. A. (2005) Zinc hydrolases: The mechanisms of zinc-dependent deacetylases, *Arch. Biochem. Biophys. 433*, 71−84.
7. Clements, J. M., Coignard, F., Johnson, I., Chandler, S., Palan, S., Waller, A., Wijkmans, J., and Hunter, M. G. (2002) Antibacterial activities and characterization of novel inhibitors of LpxC, *Antimicrob. Agents Chemother. 46*, 1793−1799.
8. Pirrung, M. C., Tumey, L. N., McClerren, A. L., and Raetz, C. R. H. (2003) High-throughput catch-and-release synthesis of oxazoline hydroxamates. Structure-activity relationships in novel inhibitors of Escherichia coli LpxC: In vitro enzyme inhibition and antibacterial properties, *J. Am. Chem. Soc. 125*, 1575−1586.
9. Kline, T., Andersen, N. H., Harwood, E. A., Bowman, J., Malanda, A., Endsley, S., Erwin, A. L., Doyle, M., Fong, S., Harris, A. L., Mendelsohn, B., Mdluli, K., Raetz, C. R. H., Stover, C. K., Witte, P. R., Yabannavar, A., and Zhu, S. G. (2002) Potent, novel in vitro inhibitors of the Pseudomonas aeruginosa deacetylase LpxC, *J. Med. Chem. 45*, 3112−3129.
10. Pirrung, M. C., Tumey, L. N., Raetz, C. R. H., Jackman, J. E., Snehalatha, K., McClerren, A. L., Fierke, C. A., Gantt, S. L., and Rusche, K. M. (2002) Inhibition of the antibacterial target UDP-(3-O-acyl)-N- acetylglucosamine deacetylase (LpxC): Isoxazoline zinc amidase inhibitors bearing diverse metal binding groups, *J. Med. Chem. 45*, 4359−4370.
11. Li, X. C., Uchiyama, T., Raetz, C. R. H., and Hindsgaul, O. (2003) Synthesis of a carbohydrate-derived hydroxamic acid inhibitor of the bacterial enzyme (LpxC) involved in lipid A biosynthesis, *Org. Lett. 5*, 539−541.
12. Jackman, J. E., Fierke, C. A., Tumey, L. N., Pirrung, M., Uchiyama, T., Tahir, S. H., Hindsgaul, O., and Raetz, C. R. H. (2000) Antibacterial agents that target lipid A biosynthesis in Gram-negative bacteria: Inhibition of diverse UDP-3-O-(R-3-hydroxymyristoyl)-N-acetyglucosamine deacetylases by substrate analogs containing zinc binding motifs, *J. Biol. Chem. 275*, 11002−11009.
13. Supuran, C. T., Casini, A., and Scozzafava, A. (2003) Protease inhibitors of the sulfonamide type: Anticancer, antiinflammatory, and antiviral agents, *Med. Res. Rev. 23*, 535−558.
14. Leung, D., Abbenante, G., and Fairlie, D. P. (2000) Protease inhibitors: Current status and future prospects, *J. Med. Chem. 43*, 305−341.
15. Supuran, C. T., Scozzafava, A., and Casini, A. (2003) Carbonic anhydrase inhibitors, *Med. Res. Rev. 23*, 146−189.
16. Whittington, D. A., Rusche, K. M., Shin, H., Fierke, C. A., and Christianson, D. W. (2003) Crystal structure of LpxC, a zinc-dependent deacetylase essential for endotoxin biosynthesis, *PNAS 100*, 8146−8150.
17. Coggins, B. E., Li, X. C., McClerren, A. L., Hindsgaul, O., Raetz, C. R. H., and Zhou, P. (2003) Structure of the LpxC deacetylase with a bound substrate-analog inhibitor, *Nat. Struct. Biol. 10*, 645−651.
18. Coggins, B. E., McClerren, A. L., Jiang, L., Li, X., Rudolph, J., Hindsgaul, O., Raetz, C. R. H., and Zhou, P. (2005) Refined solution structure of the LpxC-TU-514 complex and p*K*a analysis of an active site histidine: Insights into the mechanism and inhibitor design, *Biochemistry 44*, 1114−1126.
19. Gennadios, H. A., Whittington, D. A., Li, X., Fierke, C. A., and Christianson, D. W. (2006) Mechanistic inferences from the binding of ligands to LpxC, a metal-dependent deacetylase, *Biochemistry 45*, 7940−7948.
20. Young, K., Silver, L. L., Bramhill, D., Cameron, P., Eveland, S. S., Raetz, C. R. H., Hyland, S. A., and Anderson, M. S. (1995) The envA permeability cell division gene of Escherichia coli encodes the second enzyme of lipid A biosynthesis: UDP-3-O-(R- 3-hydroxymyristoyl)-N-acetylglucosamine deacetylase, *J. Biol. Chem. 270*, 30384−30391.
21. McClure, C. P., Rusche, K. M., Peariso, K., Jackman, J. E., Fierke, C. A., and Penner-Hahn, J. E. (2003) EXAFS studies of the zinc sites of UDP-(3-O-acyl)-N- acetylglucosamine deacetylase (LpxC), *J. Inorg. Biochem. 94*, 78−85.
22. Sorensen, P. G., Lutkenhaus, J., Young, K., Eveland, S. S., Anderson, M. S., and Raetz, C. R. H. (1996) Regulation of UDP-3-0- R-3-hydroxymyristoyl-N-acetylglucosamine deacetylase in Escherichia coli: The second enzymatic step of lipid a biosynthesis, *J. Biol. Chem. 271*, 25898−25905.
23. Okuyama, K., Hamamoto, T., Ishige, K., Takenouchi, K., and Noguchi, T. (2000) An efficient method for production of uridine 5′-diphospho-N-acetylglucosamine, *Biosci. Biotechnol. Biochem. 64*, 386−392.
24. Leiting, B., Pryor, K. D., Eveland, S. S., and Anderson, M. S. (1998) One-day enzymatic synthesis and purification of UDP-N-[1-C-14]acetyl-glucosamine, *Anal. Biochem. 256*, 185−191.
25. Harris, D. C. (1996) *Quantitative Chemical Analysis*, 4th ed., W. H. Freeman and Company, New York.
26. Benson, J. R., and Hare, P. E. (1975) Ortho-phthalaldehyde: Fluorogenic detection of primary amines in picomole range—Comparison with fluorescamine and ninhydrin, *Proc. Natl. Acad. Sci. U.S.A. 72*, 619−622.
27. McClerren, A. L., Zhou, P., Guan, Z., Raetz, C. R. H., and Rudolph, J. (2005) Kinetic analysis of the zinc-dependent deacetylase in the lipid A biosynthetic pathway, *Biochemistry 44*, 1106−1113.
28. Jackman, J. E., Raetz, C. R. H., and Fierke, C. A. (2001) Site-directed mutagenesis of the bacterial metalloamidase UDP-(3-O-acyl)-N-acetylglucosamine deacetylase (LpxC). Identification of the zinc binding site, *Biochemistry 40*, 514−523.
29. Blasko, A., Bunton, C. A., Bunel, S., Ibarra, C., and Moraga, E. (1997) Determination of acid dissociation constants of anomers of amino sugars by 1H NMR spectroscopy, *Carbohydr. Res. 298*, 163−172.
30. Robitaille, P. M. L., Robitaille, P. A., Brown, G. G., and Brown, G. G. (1991) An analysis of the Ph-dependent chemical-shift behavior of phosphorus-containing metabolites, *J. Magn. Reson. 92*, 73−84.
31. Beall, B., and Lutkenhaus, J. (1987) Sequence-analysis, transcriptional organization, and insertional mutagenesis of the envA gene of Escherichia coli, *J. Bacteriol. 169*, 5408−5415.
32. Normark, S., Boman, H. G., and Matsson, E. (1969) Mutant of Escherichia coli with anomalous cell division and ability to decrease episomally and chromosomally mediated resistance to ampicillin and several other antibiotics, *J. Bacteriol. 97*, 1334−1342.
33. Nishio, M., Umezawa, Y., Hirota, M., and Takeuchi, Y. (1995) The CH/p interaction: Significance in molecular recognition, *Tetrahedron 51*, 8665−8701.
34. Sujatha, M. S., and Balaji, P. V. (2004) Identification of common structural features of binding sites in galactose-specific proteins, *Proteins: Struct., Funct., Genet. 55*, 44−65.
35. Sujatha, M. S., Sasidhar, Y. U., and Balaji, P. V. (2004) Energetics of galactose- and glucose-aromatic amino acid interactions: Implications for binding in galactose-specific proteins, *Protein Sci. 13*, 2502−2514.
36. Mildvan, A. S., Weber, D. J., and Kuliopulos, A. (1992) Quantitative interpretations of double mutations of enzymes, *Arch. Biochem. Biophys. 294*, 327−340.
37. Mildvan, A. S. (2004) Inverse thinking about double mutants of enzymes, *Biochemistry 43*, 14517−14520.
38. Weber, D. J., Meeker, A. K., and Mildvan, A. S. (1991) Interactions of the acid and base catalysts on Staphylococcal nuclease as studied in a double mutant, *Biochemistry 30*, 6103−6114.
39. Hernick, M., and Fierke, C. A. (2006) Molecular recognition by *E. coli* UDP-3-O-(R-3-hydroxymyristoyl)-N-acetylglucosamine deacetylase is modulated by bound metal ions, in press.
40. Li, X. C., McClerren, A. L., Raetz, C. R. H., and Hindsgaul, O. (2005) Mapping the active site of the bacterial enzyme LpxC using novel carbohydrate-based hydroxamic acid inhibitors, *J. Carbohydr. Chem. 24*, 583−609.

BI061405K